AFRL-AFOSR-VA-TR-2022-0692

Developing Methods of Control of Self-Organized Plasma Structures in Devices Relevant to Electric Propulsion

Raitses, Yevgeny
TRUSTEES OF PRINCETON UNIVERSITY
1 NASSAU HALL
PRINCETON, NJ,
US

09/28/2022
Final Technical Report

Air Force Research Laboratory
Air Force Office of Scientific Research
Arlington, Virginia 22203
Air Force Materiel Command

REPORT DOCUMENTATION PAGE

PLEASE DO NOT RETURN YOUR FORM TO THE ABOVE ORGANIZATION.

1. REPORT DATE	2. REPORT TYPE	3. DATES COVERED	
		START DATE	END DATE
20220928	Final	20170201	20210228

4. TITLE AND SUBTITLE
Developing Methods of Control of Self-Organized Plasma Structures in Devices Relevant to Electric Propulsion

5a. CONTRACT NUMBER	5b. GRANT NUMBER	5c. PROGRAM ELEMENT NUMBER
	FA9550-17-1-0010	61102F

5d. PROJECT NUMBER	5e. TASK NUMBER	5f. WORK UNIT NUMBER

6. AUTHOR(S)
Yevgeny Raitses

7. PERFORMING ORGANIZATION NAME(S) AND ADDRESS(ES)
TRUSTEES OF PRINCETON UNIVERSITY
1 NASSAU HALL
PRINCETON, NJ
US

8. PERFORMING ORGANIZATION REPORT NUMBER

9. SPONSORING/MONITORING AGENCY NAME(S) AND ADDRESS(ES)	10. SPONSOR/MONITOR'S ACRONYM(S)	11. SPONSOR/MONITOR'S REPORT NUMBER(S)
Air Force Office of Scientific Research 875 N. Randolph St. Room 3112 Arlington, VA 22203	AFRL/AFOSR RTA1	AFRL-AFOSR-VA-TR-2022-0692

12. DISTRIBUTION/AVAILABILITY STATEMENT
A Distribution Unlimited: PB Public Release

13. SUPPLEMENTARY NOTES

14. ABSTRACT
The research conducted under this project was built upon advances in understanding of plasma instabilities and relevant kinetic effects responsible for anomalous electron cross-field transport and associated mode transition with and without plasma structures in a simplified uniform E×B plasma configuration of the Penning plasma discharge. The overall goal of the project was to apply this unique knowledge and developed experimental and modeling tools to more complex magnetized configurations operating under more realistic conditions encountered in plasma propulsion devices, including effects of gas pressure, magnetic-field and plasma-pressure gradients, and the flows. Synergy effects between transport phenomena and plasma-wall interaction were also in the focus of the project. The research plan was to carry out high fidelity measurements of time-averaged and time-resolving plasma properties and perform particle-in-cell simulations which would resolve multi-dimensional and multiscale nature of plasma transport phenomena encountered in space plasma propulsion and related plasma devices. The intention was also to develop and apply effective methods of control of plasma structures and mode transition based on fundamental understanding of their mechanisms. The project was a joint collaboration between Princeton University, the DOE Princeton Plasma Physics Laboratory (PPPL), Stanford University and their associated

15. SUBJECT TERMS

16. SECURITY CLASSIFICATION OF:			17. LIMITATION OF ABSTRACT	18. NUMBER OF PAGES
a. REPORT	b. ABSTRACT	c. THIS PAGE		
U	U	U	UU	15

19a. NAME OF RESPONSIBLE PERSON	19b. PHONE NUMBER *(Include area code)*
MITAT BIRKAN	426-7234

Final Report on the Project "Developing Methods of Control of Self-Organized Plasma Structures in Devices Relevant to Electric Propulsion", FA9550-17-1-0010

Principal Investigator (PI): Yevgeny Raitses, Princeton University, Princeton, NJ 08544

Co-PI: Mark Cappelli, Stanford University, Stanford, CA 94305

Co-PI: Igor Kaganovich, Princeton Plasma Physics Laboratory, Princeton, NJ 08543

1. Introduction

Magnetized plasmas in electric propulsion devices are strongly non-equilibrium system that exhibit complex nonlinear behavior resulting in variety of (turbulent) fluctuations and related anomalous transport phenomena, and structures that critically affect the device performance, efficiency and longevity. The research conducted under this project was built upon advances in understanding of plasma instabilities and relevant kinetic effects responsible for anomalous electron cross-field transport and associated mode transition with and without plasma structures in a simplified uniform E×B plasma configuration of the Penning plasma discharge. The overall goal of the project was to apply this unique knowledge and developed experimental and modeling tools to more complex magnetized configurations operating under more realistic conditions encountered in plasma propulsion devices, including effects of gas pressure, magnetic-field and plasma-pressure gradients, and the flows. Synergy effects between transport phenomena and plasma-wall interaction were also in the focus of the project. The research plan was to carry out high fidelity measurements of time-averaged and time-resolving plasma properties and perform particle-in-cell simulations which would resolve multi-dimensional and multi-scale nature of plasma transport phenomena encountered in space plasma propulsion and related plasma devices. The intention was also to develop and apply effective methods of control of plasma structures and mode transition based on fundamental understanding of their mechanisms. The project was a joint collaboration between Princeton University, the DOE Princeton Plasma Physics Laboratory (PPPL), Stanford University and their associated collaborators.

Our research approach plan was to start the study of the above-mentioned effects for a simplified geometry devices such as ExB Penning discharges and magnetron discharges and then, proceed with the exploration of more complex configurations, including Hall thrusters. This scientific approach of progression from simple to more complex configurations proved to be effective in development of validated modeling capabilities that can be used for predictions and prototyping of future devices. A summary of our research accomplished in this project is as follows:

1. **Towards validated predictive modeling of ExB devices:**
    a. Using experiments and PIC simulations of the ExB Penning discharge, confirmed our linear theory prediction that the spoke formation is driven by the gradient-drift instability such as collisonless Simon-Hoh instability (CSHI). This instability requires the electric field and the plasma density gradient to be codirected across the magnetic field. Consistent with this condition, experiments and PIC simulations showed that the spoke is suppressed

when the magnetic field lines are terminated by the anode (similar to TAL-type Hall thruster) thereby, eliminating the electric field in the plasma.

b. Predicted an inverse energy cascade in the nonlinear regime of instabilities in ExB plasma relevant to magnetized plasma spacecraft propulsion. The instability proceeds by developing a large amplitude coherent wave (e.g. spoke) driven by the energy input from the small scale fundamental cyclotron resonance. The anomalous electron transport is dominated by the long wavelength part of the turbulent spectrum (i.e. spoke).

c. We have developed a theory that confirms that in magnetron discharge, the mode of the structures undergo distinct transitions, with higher order modes favored at lower discharge voltage. The theory is similar to that developed to understand low frequency disturbances seen in Hall thrusters. Our theory included plasma diffusion along the magnetic field, which was found to expand the domain of instability. We showed that the model can account for the dispersion seen in our experiments, and it predicts the retrograde rotation, i.e., the rotation opposite the **E** x **B** drift.

d. Advanced in fully kinetic self-consistent 2-D Particle-in-Cell simulations of real size ExB plasma devices of cylindrical geometry. For the first time, achieved simulations time-scale comparable with low frequency (10's kHz) spoke and breathing oscillations observed in these discharges and Hall thrusters. Simulations of ExB Penning discharge demonstrated that the spoke provides enhanced (anomalous) electron transport in good agreement with the experimental data.

2. **Control of coherent structures in the Hall thruster:** Developed and demonstrated active control of plasma structures including rotating spoke and breathing oscillations with applications to 1) waveguide devices for the control of electromagnetic waves and 2) magnetized plasma thrusters.

   a. Demonstrated experimentally that the azimuthally (ExB) rotating spoke mode in the cylindrical Hall thruster can be suppressed by the external modulation of the anode voltage at frequencies near the natural breathing mode. These results show that there is an interaction between the spoke and breathing (axial) modes. Since the spoke is driven by the axial gradients of the plasma density and the plasma potential (axial electric field), changes in these gradients caused by breathing oscillations may alter the spoke.

   b. Using the developed 1-D fluid model of the Hall thruster with externally modulated anode voltage proposed an explanation for an increase of the beam efficiency. This increase was observed in our previous experiments when the modulation frequency was near the natural breathing mode. The model predicts that the external modulation drives oscillations of both the ion velocity and the plasma density closer in phase increasing the total ion current. This prediction is consistent with more recent experiments.

   c. Demonstrated a novel approach of suppression of low frequency beathing instabilities and the mitigation of the anomalous cross field transport by adding segmented electrodes to a wall-less Hall thruster (inverse magnetron configuration) with potentially longer lifetime than conventional annular and cylindrical Hall thrusters and more suitable for scaling down to operate at low powers. The thruster with segmented electrodes demonstrated a narrower plume and higher efficiencies at the power levels < 200 W

d. Demonstrated the fastest ExB rotating spoke (~ 100 MHz) which can be relevant for plasma-based control of electromagnetic waves. This result was achieved for the magnetron discharge operating with helium gas. Important for this application, the spoke frequency can be varied by changing the working gas from the slowest spoke of ~ 10's kHz for xenon to the fastest spoke for helium. The measured dependence of the spoke frequency on the ion mass tends to follow a general trend consistent with theoretical dependence for the instability ~ $(M_{ion})^{-0.5}$.

In the following sections, we highlight key results of our studies in the last year of this project.

2. Control of ExB plasma using segmented electrodes in a Hall thruster (Princeton/PPPL)

It was experimentally demonstrated that the use of biased segmented electrodes (active boundaries of the plasma) can allow the mitigation of large amplitude breathing oscillations in Hall thrusters, the reduction of the electron cross-field transport, and the plume narrowing leading to an increase of the thrust. These remarkable effects were measured for the wall-less Hall thruster,[1,2] which resembles an inverse magnetron configuration. In the absence of the channel walls bounding the plasma, a wall-less Hall thruster is a promising configuration with a potentially longer lifetime and easier scalability than conventional Hall thrusters. In the wall-less Hall thruster, a fringing-kind magnetic field topology with a strong axial component of the magnetic field (Fig. 1) leads to the formation of radial electric fields, which accelerates ions out of the thruster radially. This causes plasma plume divergence and a reduction in thrust. In previous works, plume narrowing effects for annular and cylindrical Hall thrusters using segmented electrodes[3] and a plasma lens[4] have been demonstrated. In this work, we apply this approach to the wall-less Hall thruster,[2] which has a different ExB configuration, but still obtains similar narrowing of the plume. The result suggests this method to be a generalized approach to plume narrowing in such ExB plasma sources and thrusters. Moreover, we also report an unexpected effect of the segmented electrode on electron-cross field current and the breathing mode, leading to additional improvements of thruster performance. The breathing mode is a commonly reported plasma instability in Hall thrusters which manifests as high-amplitude, low frequency (~10 kHz) discharge current oscillations due to the periodic ionization of neutral propellant.[5]

The principle of operation of the wall-less thruster is expected to be generally similar to that of conventional Hall thrusters. One of key differences is in the enhanced role of the magnetic mirror at the center of the wall-less thruster which forms a magneto-electrostatic trap (MET)[1] for electrons bouncing between the mirror and the plasma plume, which is at nearly the cathode potential. A key difference of the MET thruster utilized in this

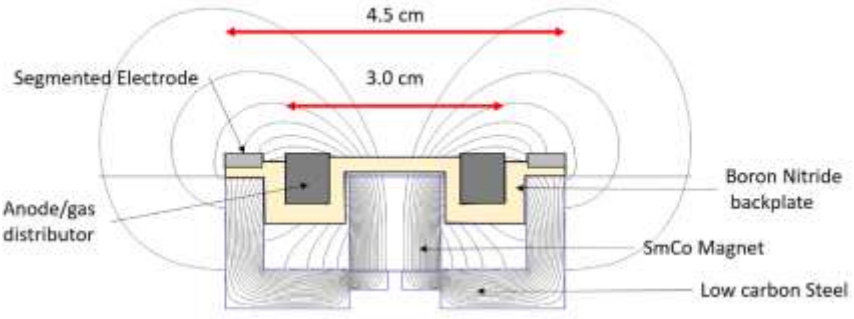

Fig. 1: Schematic and magnetic field lines of the segmented wall-less Hall thruster. Cathode-neutralizer is placed outside the thruster in the near plume and is not shown on this figure.[5]

study from the other wall-less thrusters is the additional low magnetic-permeability stainless-steel electrode placed along the thruster edge, with magnetic field lines connecting the electrode and the center of the thruster (Fig. 1). This placement of the electrode was selected to implement a plasma lens effect[4] on the ions by increasing the plasma potential around the thruster edge to straighten outward-bound ions and lower plume divergence. This electrode is biased by a separate power supply with a variable voltage with respect to the cathode. Note that segmented electrode here refers to an electrode segmented radially from the anode, whereas previous uses of the term segmented electrodes have referred to electrodes segmented axially.[3]

The thruster was operated in the vacuum facility described elsewhere.[3] All experiments were conducted with xenon gas. The gas flow rate through the anode was 4, 6 and 8 sccm. A commercial hollow cathode was used as the cathode-neutralizer. The cathode flow rate was constant at 2 sccm. The discharge voltage between the thruster anode and the thruster cathode was 250V. The bias voltage applied to the segmented electrode was varied. During the described experiments, the background gas pressure did not exceed 3 x 10^{-6} Torr. Finally, for diagnostics, we used a high resolution (±0.1 mN) thrust stand and plume diagnostics which are described elsewhere.[6]
Experiments demonstrated that the wall-less thruster exhibits a significant breathing mode of discharge current oscillations with amplitudes above 30% of the mean value. As the segmented electrode voltage increases from the floating value of +20V with respect to the cathode, the amplitude of the breathing mode decreases to ~5%, particularly when the bias voltage is about 100V (Fig. 2). Moreover, at the low flow rate of 4 sccm, a strong breathing mode caused unstable operation of the thruster. Stable operation at this flow rate was only possible with a voltage of at least 70 V applied to the segmented electrode.

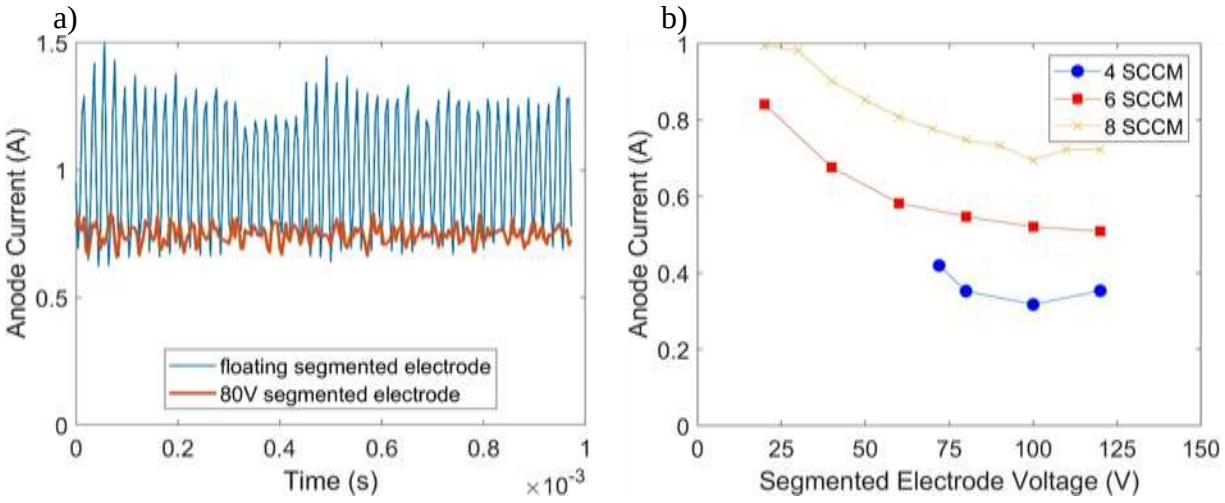

Fig. 2: Suppression of the breathing mode due to the bias of the segmented electrode shown by (a) anode current traces for 8 sccm mass flow and (b) Decrease in the anode current with the segmented electrode bias voltage. Note that the current through the segmented electrode increases with the bias voltage

This remarkable mitigation of the breathing mode was correlated with a decrease of the discharge current (Fig. 2b). and an increase of current through the segmented electrode.[2] Interestingly, as the segmented electrode voltage increased above ~100V, strong discharge current oscillations (Fig. 2a) appeared again. In these regimes, the thruster discharge becomes extremely unstable.

Regarding the suppression of the breathing oscillations observed at the certain bias voltages of the segmented electrode (~ 80 V), our hypothesis is that this is a result of the competition between the main thruster discharge and the segmented electrode discharge. Large amplitude oscillations of the discharge current (Fig. 2a) occur when the feedstock of neutral atoms or plasma density is depleted over an oscillation. When the majority of the current is through one electrode, the frequency of the breathing oscillations is set by the geometry and plasma properties of the associated region and the oscillations occur coherently. However, once the current is split between the two electrodes, there are two paths for the excess electrons generated by the breathing mode. The difference in the natural breathing mode frequencies in these discharges allows a persistent electron supply to be maintained, as electrons can diffuse between the outer electrode and anode region. This inhibits the buildup of the neutral density (and its perturbation due to wall recombination of the backflow ions) and prevents the growth of the ionization instability which gives rise to large amplitude oscillations of the discharge current. The above phenomenological description can hint at an explanation towards why the frequency is constant with electrode voltage on either side of the voltage band corresponding to the suppression of the breathing mode.

We also conducted measurements of the thruster performance and plasma plume in this thruster as a function of the bias voltage to the segmented electrode (Fig. 3). It could be expected that providing an alternate electrode close to the cathode may increase the discharge power, however it appears that total power decreases as the segmented electrode is applied, up to 50 W out of the nominal 210 W operation at 6 sccm (Fig. 3a). These power reductions are considerable and appeared consistently. We note that the largest decrease in power occurred for the 6sccm mass flow, which originally had a breathing mode current amplitude ~70% of the mean current. This power decreases as the current is diverted from the higher voltage anode to the lower voltage segmented electrode and increases again when this segmented electrode starts to dominate in current at high voltages.

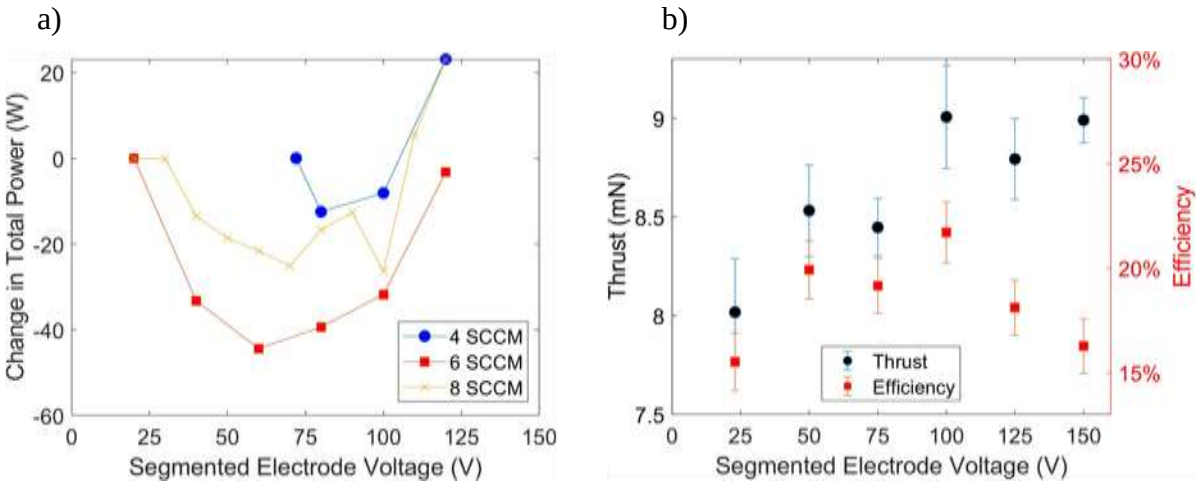

Fig. 4 Effects of the segmented electrode: a) Decrease in thruster power as the segmented electrode voltage increases from the nominal condition (4 sccm: 128 W, 6 sccm: 210 W, 8 sccm: 248 W). Thruster was unstable at 4sccm without the biased segmented electrode, and so the 70V bias was taken as the nominal power for this mass flow; b) Increase in thrust and efficiency as the segmented electrode voltage increases from the nominal condition of 250V anode voltage and 8sccm Xe mass flow rate.

Interesting, that the thrust increased up to 12% at the bias voltage corresponding to the regime with the minimum power (Fig. 3b). Measurements of the plasma plume in this regime showed some plume narrowing as the segmented electrode voltage was increased: at 8sccm the 95% plume half-angle decreased from 57° nominal to 54° at 100V segmented electrode bias. This corresponds to an expected $[\frac{\cos 54°}{\cos 57°} = 8\%]$ improvement in the thrust. Over this range the ion current in the plume remained relatively steady at 0.63 A with an associated propellant utilization of 110%, which is typical for this thruster due to multi-charged ions.[7] Similar plasma-focusing trends were observed at anode voltages of 350 V. A plasma lens generated by the altered plasma potential profile may be focusing the ions as shown in other works.[4] Another potential mechanism is the reduction in central plasma pressure. Measurements have shown high plasma pressure in the middle of this wall-less Hall thruster, and by allowing electrons to flow along the magnetic field lines from the center to the outer electrode this plasma pressure may be reduced, which would in turn reduce the associated radial electric fields.

In this work, the addition of a biased segmented electrode to the wall-less thruster is shown to significantly narrow the plasma plume and suppress large amplitude breathing oscillations of the discharge current commonly associated with ionization instability. Both effects result in improvements to the thruster performance. Physical mechanisms responsible for these effects are unclear, but they are apparently associated with the reduction of the electron cross-field transport to the anode and a transition in the breathing mode frequency. Two-dimensional or three-dimensional models are needed to fully understand the observed effects of the segmented electrode on the oscillations and performance of the thruster as the system with three electrodes (anode, segmented electrode and the cathode) and two-dimensional magnetic field topology is quite complex.

3. Advanced in understanding of ExB magnetron discharge (Stanford)

The focus of our studies was on the miniature magnetron discharges shown in Fig. 5. Measurements have been with race-track (the circular plasma region) dimensions as small as 5 mm in diameters and as large as 30 mm in diameter. The plasma ring tends to form in regions where the magnetic field is strongest, and where the B-field has a predominantly radial direction. Under varying ranges of conditions, all seem to exhibit coherent instabilities of the gradient-driven types. The magnetron shown schematically in Fig. 5 is the smallest of those we have studied. In some cases, the discharge is sustained between a graphite cathode and a transparent indium tin oxide (ITO) anode, providing direct optical access (usually the anode is a solid metal, but we use transparent conductors to visualize the plasma through high speed imaging as shown in the figure). A Co-Sm ring magnet with an iron core generates the

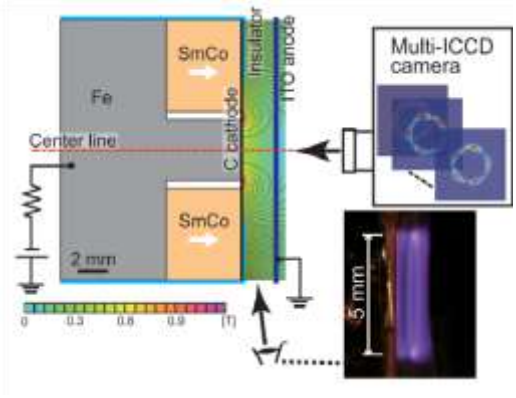

Fig. 5 Schematic of a small racetrack diameter magnetron discharge with imposed computed magnetic fields. Also shown is a photo of the plasma (side view) and a representation of camera recordings of drift instabilities.

magnetic field topology. The maximum field at the cathode is typically ~1 T. Axial gradients are generated in both the plasma density and magnetic field. As mentioned above, these gradients drive coherent rotating structures attributed to Modified Simon-Hoh type instabilities. The frequency that we see in these discharges is much higher than the rotating structures seen in larger Penning discharges and the disturbances are much more regular. For the magnetron discharge shown in Fig. 1, the dispersion seen in Fig. 6 has mode frequencies as high as 700 kHz. In the last few years, our yet unpublished studies have indicated that the larger magnetron discharges of similar designs tend to have higher mode frequencies even at similar discharge gap dimensions.

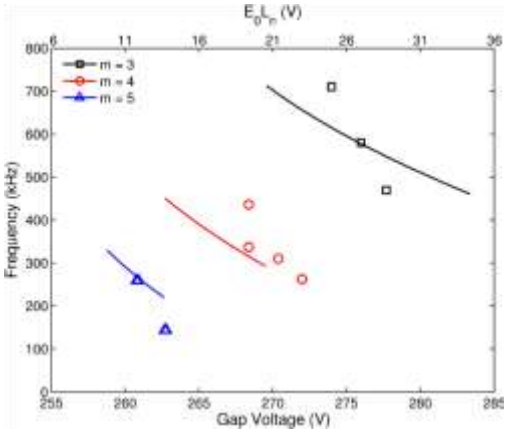

Fig. 6 Measured and predicted rotation frequency vs. voltage during retrograde motion. The value m is the mode number, $m = kR$, with R is the radius of the plasma ring, and k the wavenumber of the disturbances. Here, E_o is the presumed local reversed field, and L_n the density gradient length scale.

High Speed Videography

We have characterized this larger magnetron discharge using high speed videography to identify the coherent plasma structures and map their dispersion (Fig. 7). Using an image intensified ultra-high speed camera (Shimadsu HPX-2 with LaVision intensifier) capable of capturing 256 full video frames at a rate of 10 million frames per second, we have confirmed that under a range of conditions (described further, below), this discharge

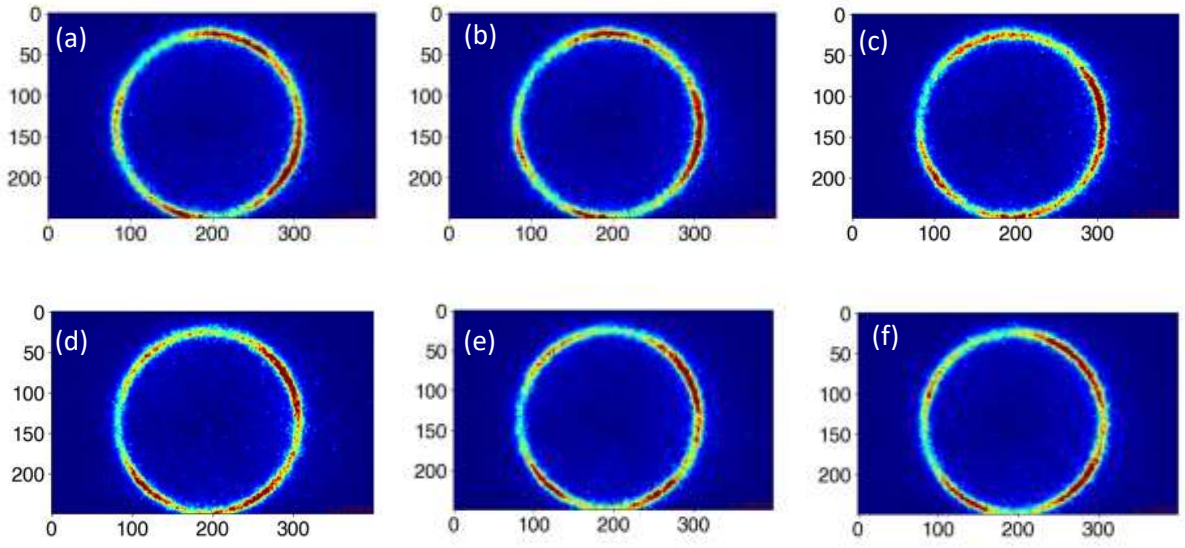

Fig. 7 A series of frames extracted from a 256-frame image intensified video of the magnetron discharge plasma as viewed through a transparent anode. The video is recorded using an intensified Shimadsu HPV-2 camera operating at 10 MHz framing rate with a 50 ns gate, 100 ns apart.

exhibits retrograde rotating and very coherent drift wave instabilities. Six frames extracted from a 256 frame video are shown in Fig. 7. Here, the **E** x **B** direction is clockwise, however, a close inspection of the images, together with the analysis of segmented anode section currents (discussed below) indicates that the plasma structure rotation is retrograde in its rotation, and, in this particular case has a mode number ($m = kR$) of 4.

I-V Characteristics

A unique feature of this device is that at low discharge current the V-I curve shows a *negative resistance coefficient* (Fig. 8). We believe this to be another (indirect) proof of the electric field inversion hypothesis. The inverted field in the region of formation of the instability, which is the region of higher plasma density, leads to an anomalous flux of ions towards the anode which contributes negatively to the total current. Moreover, since the value of the inverted electric field is higher at low currents, due to the higher plasma confinement, it stands to reason that this anomalous ion flux is maximum at lower currents and decreases with an increase of currents, until the field reverses and the electrical resistance becomes positive. This nonlinear phenomenon leads to two possible states at same discharge voltage, depending on the history of the current. The difference in currents between the two states is the current anomaly and, for the reason mentioned above, is maximum at low discharge current. The existence of these two distinctly different states of the discharge is in of itself an interesting phenomenon that deserves further study.

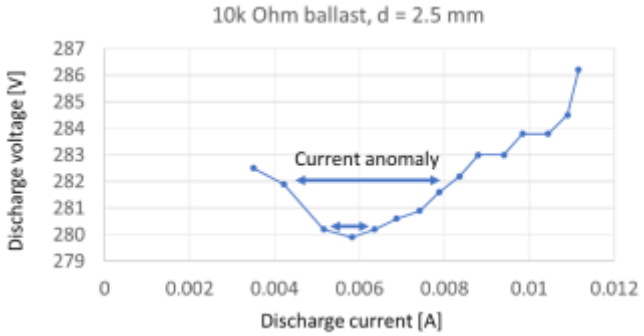

Fig. 8 A typical V-I characteristic seen in these small magnetron discharges. The presence of a negative resistance is hypothesized to be further evidence and indicative of a field reversal within the gap.

Our theoretical models [8, 9] have suggested that at low currents, the high magnetic confinement of electrons leads to large plasma density gradients which are responsible for the field inversion. However, at higher currents, the Bohm diffusion of electrons across the magnetic field dominates, leading to lower plasma confinement and hence lower plasma gradients. For this reason, at high currents, the conditions of field inversion are not met, and the rotation is in the usual **E** x **B** direction. This threshold current is dependent on the distance between the electrode (reference threshold current is 6 mA). In our smaller and larger magnetron device, the instability loses the coherent state at high currents, so the rotation reversal cannot be detected by the camera. Complimentary measurements that characterize the plasma structure dynamic rotation are necessary, such as the use of a segmented anode, which proved informative in our previous studies of a much smaller discharges [8].

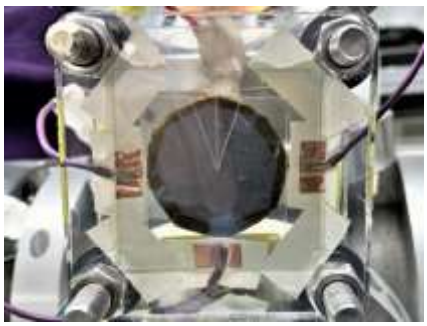

Fig. 9 Segmented anode with two laser-cut 20 degree segments and a main 320 degree segment.

We have already obtained preliminary complimentary data confirming retrograde rotation in this larger discharge by fabricating ITO anodes with laser etched separations that define individual adjacent current-collecting segments. A front view photo of the 2.5 cm diameter racetrack magnetron (the graphite covered magnetic structure is apparent) is shown in Fig. 9. One can also see in this figure, the segmented ITO anode. In this particular anode, there are three sections of collected anode current (two 15^{o} segments straddling the 12-o'clock position, and the other comprising the rest of the anode). In other designs, we have had as many as five segments of varying resolution. The anode segment data will reinforce and confirm that seen in the video, albeit with less resolution, and also provides rotation confirmation when video data is not able to be collected, such as when the discharge is operated at the PCRF center at PPPL.

Segmented Anode Confirmation

Anode segmentation allows for localized current measurements. The segments collect the anode current on angular regions along the circular plasma trace. With a designed angular separation between the segments, we can deduce useful information about the propagating instability. The angle of the segments is the distance between the locations where the current is measured and determines the spatial resolution. For example, 10-degree segments have a maximum resolution of 18 spokes and allow for detection secondary waves (i.e., higher harmonics). High-sampling speed (2 Gs/s) oscilloscopes are used to collect the segment current traces, and high-bandwidth voltage probes are used to capture the applied potentials across the gaps. A photograph of the transparent ITO anode with etched segments is shown in Fig. 9.

As an example of the data generated using wavelet analysis of the collected segmented current waveforms and their ability to confirm rotation direction, we show in Fig. 7 two cases, for conditions within the V-I characteristics presented in Fig. 8. The first case is that of high discharge current (>6mA) and hence, high current density, see Fig. 10 (a). In the spectrum of the signal at these high currents, the main azimuthal mode has a mode number of m = 4 and a main frequency of about 1.7 MHz. In these plots, positive mode numbers indicate clockwise rotation, i.e., in the positive **E** x **B** direction. At higher frequencies, within the Nyquist limit, the power of the spectrum is detected in the negative mode number region, suggesting that rotating

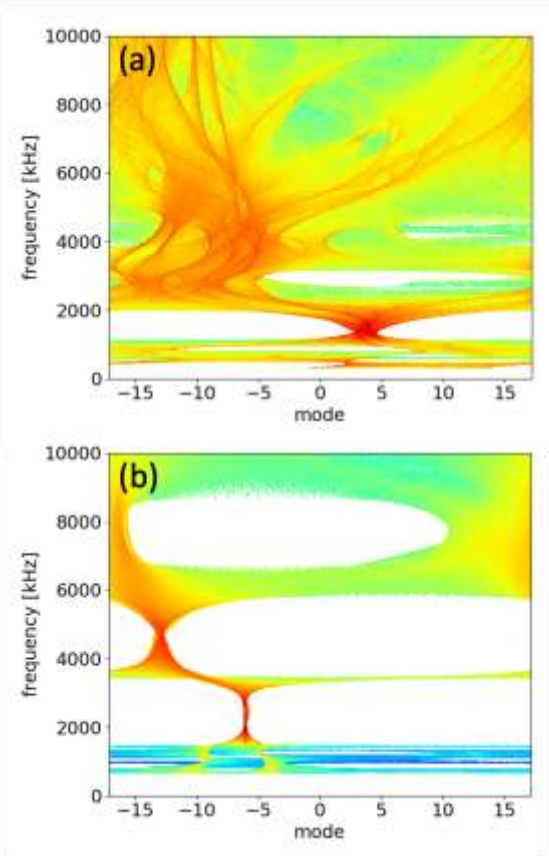

Fig. 10. Spectral dispersion maps acquired with segmented anode (a) high currents (>6mA) – dominant mode is 4 and rotates in the **E** x **B** direction at a frequency of about 1.7 MHz; (b) low current (< 6mA) – dominant mode is 7 and rotates in the *negative* **E** x **B** direction at a frequency of about 2.3 MHz.

and counter-rotating modes might co-exist, or possibly, may be intermittent. This higher frequency disturbance is noticeably less coherent.

The second case is that of a low current (< 6mA), see Fig. 10(b). Here, the main mode is seen to be m = 7 and its frequency is about 2.3 MHz. By comparison with the main feature in Fig. 10(a), this m = 7 mode is very coherent, and is propagating in the counter-clockwise (-**E** x **B**) direction. Because of the strong coherence of this m = 7 mode, a second mode can be seen at twice the main frequency (second harmonic), also within the Nyquist limit.

In our recent theoretical analysis [9] we showed how the analysis of the spectrum generated by the anode current measurements reveals the presence of disturbances at higher frequencies and wave numbers not detected in high speed video. In some cases, Fast Fourier Transforms show that these higher frequencies to be multiples (i.e., harmonics) of the main frequency (first harmonic). As shown in Fig. 10(b) above, we see these higher harmonics. In other cases, we see frequencies and mode numbers that are not harmonics and at higher frequencies (as in Fig. 10(a)). Using wavelet decomposition, as illustrated in Fig. 8(a), we find that these frequencies do not coexist, but are instead intermittent. We can see how modes labeled A, B and C, while all present in the spectrum of Fig. 11(b), are not simultaneous (the spectrum in Fig. 11(b) is uses the entire time trace, while wavelet decomposition allows for time-resolved frequency transform of each signal trace).

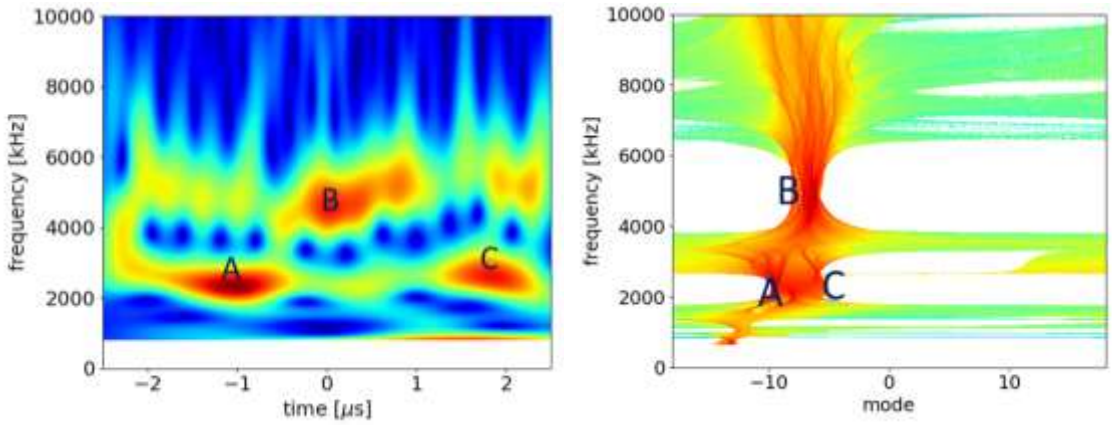

Fig. 11 (left) Wavelength decomposition of representative current traces from the segmented anode showing intermittent modes. (right) Spectrum of the entire time trace of the figure to the left.

Simulations

The experimental results motivated us to numerically solve for the spectrum of instabilities within the nonlinear stage of growth which we neglected in our linear analysis. We have constructed a numerical model that uses fourth-order numerical approximations for the derivatives to solve the non-linear amplitudes presented in Ref. [9]. Additional hyper-viscosity terms are added to the equations to numerically limit the growth of the instability and reach a saturated state.

Although the analysis is still in an early stage (we plan to submit our findings for peer review before the end of 2021), initial results show growth of harmonics, for example, when an initial m = 4 mode is used as an initial. Figure 12 (left panel) shows the predicted spatial signal at an instant in time during the non-linear phase, and Fig. 12 (right panel) is the spectrum. These harmonics, of

course, are a consequence of the periodic boundary conditions that are used to model the circularly rotating spokes, however, in the absence of non-linearities, do not appear in the numerical solution. At this time, we are carrying out simulations for the range of operations tested in the experiments for both the small and larger magnetron devices.

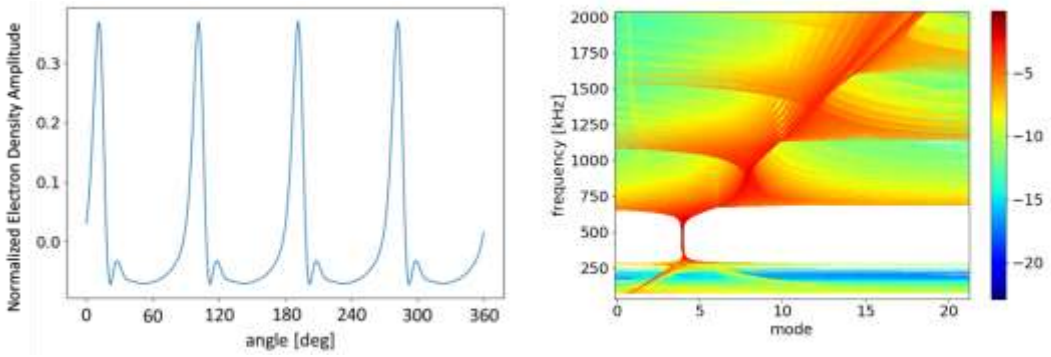

Fig. 12 (left) Normalized amplitude at a point in time (45 ms) following initial seeding of a sinusoidal m = 4 disturbance. (right) Spectrum of the entire time trace showing higher harmonics.

Verifying PPPL Particle-in-Cell Software via Kinetic Modelling of a Hall Thruster Channel (PPPL)

The Landmark project [10] is a coordinated effort led by an international cohort of developers to create software benchmarks relevant to the modelling of low-temperature plasma devices, particularly electric propulsion systems. The project aims to verify the implementation of modelling tools used by each member of the project, as well as provide a pathway for future developers to verify their own software. Several benchmarks have been developed, including for fluid, hybrid and kinetic plasma simulations. Developers from the Princeton Plasma Physics Laboratory (PPPL) have been involved in the project to validate a new kinetic particle-in-cell (PIC) code being designed to specifically target low-temperature plasma applications.

The *Low-Temperature Plasma PIC* code (LTP-PIC) has been designed to harness the power of the latest supercomputing architectures for the modelling of large-scale kinetic plasma physics problems as well as prototyping of plasma devices. The software is designed from the ground up for scalability and is accelerated via GPUs. A particular emphasis has been placed on implementing highly scalable linear algebra packages for inverting Poisson's equation and obtaining the electrostatic field, as well as Monte-Carlo models for capturing the complex collisional phenomena which can play a dominant role in low-temperature plasmas physics. The code is flexible and can model complex geometry in two and three dimensions.

The Landmark 2a benchmarking model for kinetic plasma codes is designed to be relatively simple to implement, while also capturing some aspects of the interesting physics which develop within the ion acceleration region of a Hall thruster. The model is a modified version of that first studied by *Boeuf & Garrigues* [11], wherein the researchers captured the development of electron drift instabilities occurring within a two-dimensional axial-azimuthal slice of a Hall thruster channel. These instabilities are of particular interest since they are suspected to play an important role in the anomalously high rate of cross field electron transport from the thruster cathode to anode.

Full details of the benchmark setup can be found in *Charoy et al* [12], however we provide a brief description here: the model considers an "unwrapped" two-dimensional axial-azimuthal section of a Hall thruster ion acceleration region, whereby Cartesian, rather than cylindrical coordinates are used. Figure 1 (top) shows the simulation setup. Axially (x-direction) the domain is 2.5 cm long with a 200 V potential applied between the anode and "virtual" cathode. The virtual cathode is created by reinjection of electrons 1mm from the right-hand edge of the simulation, preventing formation of a non-physical sheath at this boundary. The azimuthal direction (y-direction) is 1.28 cm long with periodic boundary conditions. No collisions are modelled, but rather electrons and Xenon ions are injected to model "ionization", Fig. 13 (bottom) shows the injection profile (red curve). While this means that certain low-frequency ionization instabilities do not emerge, it reduces ambiguity in the choice of collision algorithms between codes and significantly reduces time to a quasi-steady state solution, both important properties for a benchmark simulation. A "radial" magnetic field (z-direction, not modelled) is applied with profile shown by the blue curve in Figure 1 (bottom). The simulation is run for a total of 20 microseconds with all relevant plasma length and time scales being adequately resolved.

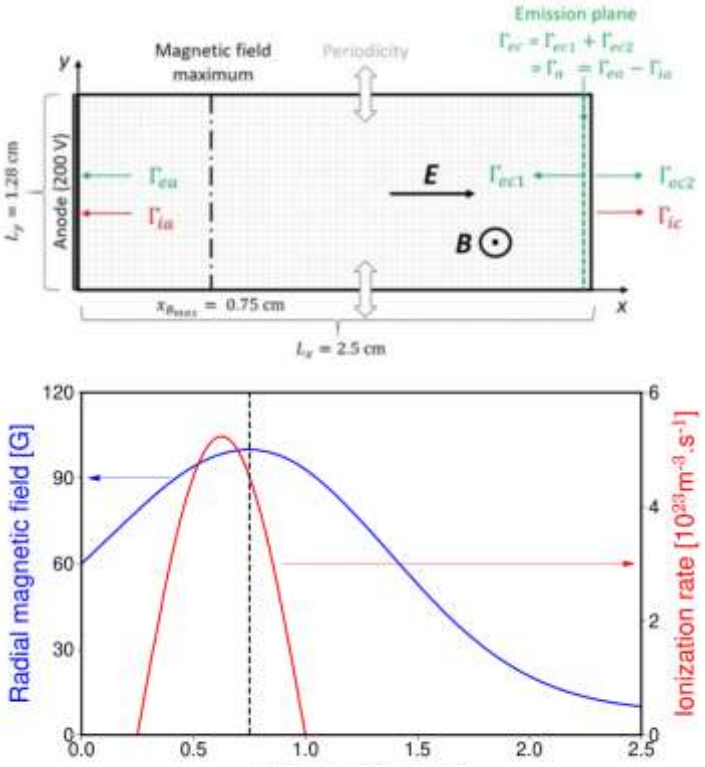

Fig. 13 (top) Simulation domain, with directions of electric, magnetic fields and currents, (bottom) applied magnetic field and ionization profiles.

Shortly after the simulation commences, high frequency azimuthal instabilities develop on the anode side of the peak magnetic field intensity (left of dashed line in Fig. 14), with lower frequency instabilities developing downstream (right of dashed line in Figure 3). While research into the exact mechanism of these instabilities is ongoing, it is suspected that they are a form of electron-cyclotron drift instability and play a critical role in enhancing electron transport across the applied magnetic field.

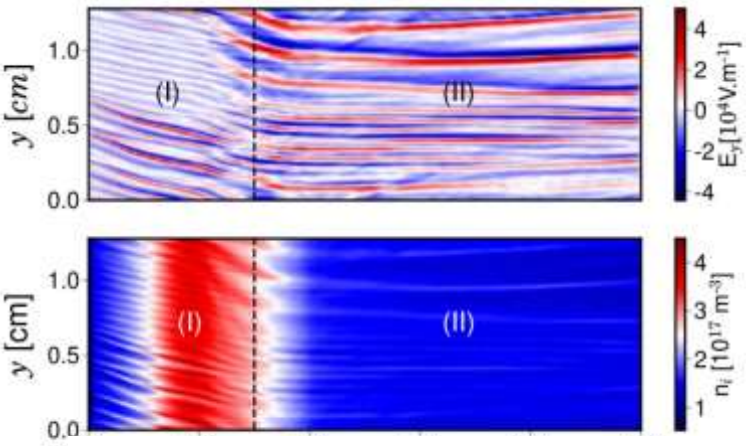

Fig. 14 Azimuthal electron cyclotron drift instabilities at 20 μs (a) Azimuthal electric field, (b) ion density.

Each of the seven codes involved in the initial Landmark 2a effort compared time averaged profiles of electric field, ion density and electron temperature, as well as Fourier transforms of the spatial and temporal behaviour of the observed instabilities. LTP-PIC was found to be in excellent agreement with all other codes involved in the benchmark providing good verification of its implementation. Figure 15 shows only the comparison of time averaged electric field with further results provided in Reference 3. Importantly, we also found that our software outperformed all other codes involved in this benchmark. In the most computationally intensive case (with an average of 300 particle-per-cell) our simulation was from 2 to 10 times faster than our collaborators (see Table 2 in Reference 3 for more details). Due to its excellent scalability, LTP-PIC could also be brought to bear in modelling a larger azimuthal slice of the Hall thruster channel. Figure 16 shows the emergence of the electron-cyclotron drift in a 10.24 cm by 2.5 cm section of a Hall thruster channel. Proportionally increasing the computational resources applied to this problem meant that the simulation time for this larger model was equal to that of the original case. It should also be highlighted that these tests were performed with the CPU version of the software, the newer GPU version will soon be applied to this benchmark to demonstrate even further improved performance.

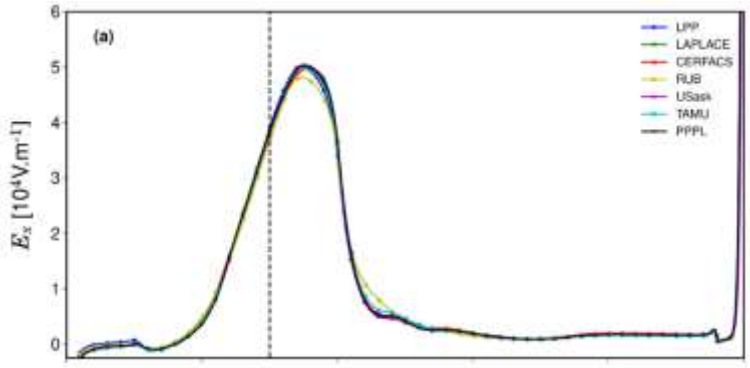

Fig. 15 Time averages ($16 - 20\ \mu s$) axial electric field profile of the 7 codes (results from LTP-PIC in black).

Through the Landmark project, the developers at PPPL were able to verify their implementation of the particle-in-cell method within the new software package, LTP-PIC. Furthermore, it was demonstrated that a well-designed and scalable software suite can exhibit superior performance, as well as open new pathways for extending low-temperature kinetic plasma simulations to significantly larger and more realistic geometries.

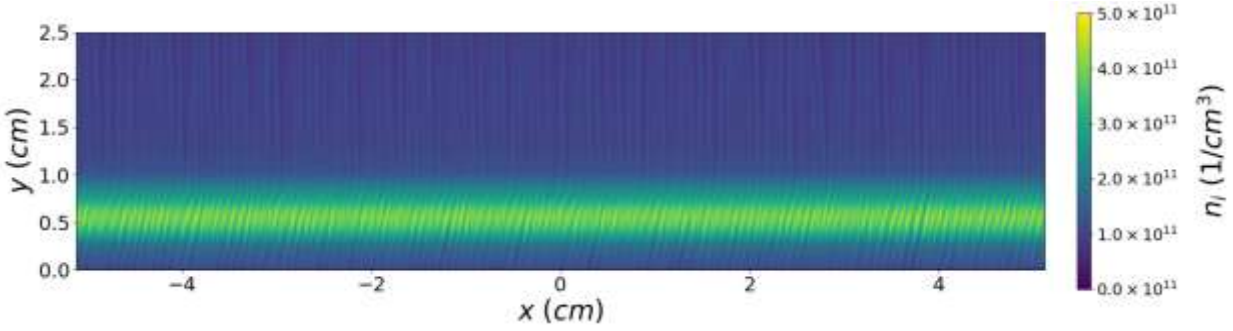

Fig. 16 Large scale axial-azimuthal simulations of a Hall thruster channel (10.24cm x 2.5 cm). Ion density at $20\ \mu s$ after the start of the simulation. Note the rotated coordinate frame compares to Figure 2, the x-direction is azimuthal, and the y-direction is axial.

References

[1] J. Simmonds and Y. Raitses, Journal of Applied Physics 130, 093302 (2021)

[2] J. Simmonds and Y. Raitses, Applied Physics Letters 119, 213501 (2021)

[3] K. D. Diamant, J. E. Pollard, R. B. Cohen, Y. Raitses, and N. J. Fisch, Propulsion and Power. 22, 1396 (2006)

[4] M. E. Griswold, Y. Raitses and N. J. Fisch, Plasma Sources Science and Technology 23, 044005 (2014)

[5] J.-P. Boeuf, J. Appl. Phys. 121, 011101 (2017)

[6] Y. Raitses, D. Staack, A. Dunaevsky, L. Dorf and N. J. Fisch, "Measurements of Plasma Flow in a 2 kW Segmented Electrode Hall Thruster", IEPC paper 03-0139, the 28th International Electric Propulsion Conference, Toulouse, France, March 2003

[7] K. Diamant, J. Pollard, Y. Raitses and N. J. Fisch, "Low Power Cylindrical Hall Thruster Performance and Plume Properties" AIAA-2008-4998, 44th AIAA/ASME/SAE/ASEE Joint Propulsion Conference and Exhibit, Hartford, CT, July 2008

[8] T. Ito, C. V. Young, and M.A. Cappelli, Applied Physics Letters 106, 254104 (2015)

[9] A. Marcovati, T. Ito, and M.A. Cappelli, Journal of Applied Physics 127, 223301 (2020)

[10] Low temperature magnetized plasma benchmarks (LANDMARK) website: https://www.landmark-plasma.com/

[11] J-P Boeuf and L Garrigues, Physics of Plasmas 25, 061204 (2018)

[12] T. Charoy et al., Plasma Sources Science and Technology 28, 105010 (2019)

Publications and Presentations

1. J. Simmonds, Y. Raitses, A. Smolyakov, and O. Chapurin, Studies of a modulated Hall thruster, Plasma Sources Science and Technology 30, 055011 (2021)

2. M. Sengupta, A. Smolyakov, and Y. Raitses, Restructuring of rotating spokes in response to changes in the radial electric field and the neutral pressure of a cylindrical magnetron plasma, Journal of Applied Physics 129, 223302 (2021)

3. M. Sengupta, A. Smolyakov, and Y. Raitses, Restructuring of rotating spokes in response to changes in the radial electric field and the neutral pressure of a cylindrical magnetron plasma, Journal of Applied Physics 129, 223302 (2021)

4. I. Kaganovich, A. Smolyakov, Y. Raitses, E. Ahedo, I. Mikellides, B. Jorns, F. Taccogna, R. Gueroult, S. Tsikata, A. Bourdon, J. P. Bouef, M. Keidar, A. Powis, M. Merino, M. Cappelli, K. Hara, J. Carlsson, N. Fisch, P. Chabert, I. Schweigert, T. Lafleur, K. Matyash, A. Khrabrov, R. Boswell, and A. Fruchtman, Physics of ExB discharges relevant to plasma propulsion and similar technologies, Physics of Plasmas 27, 120601 (2020)

5. A. Marcovati, T. Ito, and M. A. Cappelli, The dynamics of coherent modes of gradient drift instabilities in a small magnetron discharge plasma, Journal of Applied Physics, 127, 223301 (2020)

6. J. Simmonds and Y. Raitses, Theoretical Analysis of Performance Parameters in Oscillating Plasma Thrusters, Journal of Propulsion and Power 37 (4), 544 (2020)

7. T. Charoy et al., Plasma Sources Science and Technology 28, 105010 (2019)

8. E. Rodriguez, V. Skoutnev, Y. Raitses, A. Powis, I. Kaganovich, and A. Smolyakov, Boundary-induced effect on the spoke-like activity in E x B plasma, Physics of Plasmas 26, 053503 (2019)

9. O. Koshkarov, A. Smolyakov, Y. Raitses, and I. Kaganovich, Self-Organization, Structures, and Anomalous Transport in Turbulent Partially Magnetized Plasmas with Crossed Electric and Magnetic Fields, Physical Review Letters 122, 185001 (2019)

10. A. Marcovati and M. A. Cappelli, Theoretical and numerical characterization of drift-wave instabilities in magnetized discharges. APS Annual Gaseous Electronics Meeting, Virtual, Session FT3 (2020)

11. Low temperature magnetized plasma benchmarks (LANDMARK) website: https://www.landmark-plasma.com/

12. A. Marcovati and M. A. Cappelli, Experimental and Numerical Studies of Coherent and Chaotic Azimuthal Disturbances in a Magnetron Discharge. In APS Annual Gaseous Electronics Meeting Abstracts (pp. FT1-063) (2019)

13. A. Marcovati, D. Biggs, N. Gascon, M. A. Cappelli, Modulation of microwaves using rotating magnetron discharges. In APS Annual Gaseous Electronics Meeting Abstracts (pp. GT1-029) (2018)